[4]Crighton, D. G., and Huerre, P., "Shear Layer Pressure Fluctuations and Superdirective Acoustic Sources," *Journal of Fluid Mechanics*, Vol. 220, Nov. 1990, pp. 355–368.

[5]Crighton, D. G., "Computational Aeroacoustics for Low Mach Number Flows," *Computational Aeroacoustics*, Springer–Verlag, New York, 1993, pp. 50–68.

[6]Mitchell, B. E., Lele, S. K., and Moin, P., "The Direct Computation of Mach Wave Radiation in an Axisymmetric Supersonic Jet," AIAA Paper 96-1729, May 1996.

[7]Blakemore, M., Evans, G. A., and Hyslop, J., "Comparison of Some Methods for Evaluating Infinite Range Oscillatory Integrals," *Journal of Computational Physics*, Vol. 22, No. 3, 1976, pp. 352–396.

S. Glegg
Associate Editor

Crossflow Vortices of a Jet Injected into a Supersonic Crossflow

Juan Gabriel Santiago* and J. Craig Dutton†
University of Illinois at Urbana–Champaign, Urbana, Illinois 61801

Introduction

NUMEROUS investigations of the fluid mechanics of the transverse jet injected into a supersonic flow (TJISF) flowfield have been motivated by the study of supersonic combustor fuel injection, thrust vector control of rocket nozzles, and jet reaction force prediction. Early studies presented detailed qualitative discussions of the structure of the TJISF flowfield.[1,2] A few studies have provided either quantitative or semiquantitative measurements of the velocity fields of underexpanded jets injected into a supersonic flow.[3–5] Despite these investigations, there is a dearth of nonintrusive, quantitative mean velocity and turbulence measurements in the TJISF flowfield. This Note uses laser Doppler velocimetry (LDV) measurements of the mean velocity fields to study development of the crossflow vortices of a sonic, underexpanded transverse jet injected into a Mach 1.6 crossflow. These measurements add to the current understanding of this flowfield and aid in modeling efforts. This investigation is part of a larger experimental study of the mean and turbulent velocity field of a TJISF.[5]

A typical underexpanded TJISF flowfield is shown schematically in Fig. 1. The figure depicts the supersonic freestream flow with the jet injected through the bottom wall. The obstruction caused by the jet generates a bow shock in the freestream (not shown). After leaving the orifice, the jet expands through a Prandtl–Meyer fan and then compresses through a barrel shock and Mach disk. Downstream of the Mach disk, the jet plume is quickly turned downstream. Furthermore, the TJISF flowfield contains a counter-rotating crossflow vortex pair in the jet plume. This vortex action is the primary source of jet entrainment and dominates the jet's downstream velocity field.[2] Other vortical structures present in the TJISF flowfield include the horseshoe vortex that wraps around the windward side of the jet and trails downstream, shear layer vortices that form around the circumference of the jet (not shown in Fig. 1), and wake vortices periodically shed near the base of the inner jet core.

Received Aug. 9, 1996; revision received Dec. 17, 1997; accepted for publication Jan. 25, 1997.

*Graduate Research Assistant, Department of Mechanical and Industrial Engineering; currently Senior Member, Technical Staff, Spacecraft Thermal Department, The Aerospace Corporation, El Segundo, CA 90245. Member AIAA.

†Professor, Department of Mechanical and Industrial Engineering. Associate Fellow AIAA.

Experimental Facility and Diagnostics

The experiments described here used the transverse jet facility of the Gas Dynamics Laboratory at the University of Illinois at Urbana–Champaign. During the experiments, the facility's wind tunnel was run at the Mach 1.6 design condition with a stagnation pressure of 241 kPa and a stagnation temperature of 295 K (resulting in a unit $Re = 58.8 \times 10^6$ m^{-1}). A sonic, underexpanded jet with a 4-mm exit diameter (d) was injected into the test section through a window in the bottom wall of the wind tunnel. The jet stagnation pressure, stagnation temperature, jet-to-crossflow momentum flux ratio, and Reynolds number based on jet diameter for the current study are as follows: $P_{oj} = 476$ kPa, $T_{oj} = 300$ K, $J = 1.7$, and $Re_d = 1.1 \times 10^5$.

A frequency preshifted two-component LDV system was used to measure three mean velocity components, U, V, and W, as well as five of the six kinematic Reynolds stresses, $\langle u'^2\rangle$, $\langle v'^2\rangle$, $\langle w'^2\rangle$, $\langle u'v'\rangle$, and $\langle u'w'\rangle$, throughout the x–y midline plane and two y–z planes (i.e., crossflow planes; see Fig. 1). Velocity measurements were obtained at more than 4000 spatial locations with four optical setups. Also, 4000 instantaneous velocity realizations were obtained at each location to minimize statistical uncertainty. An analysis of the error associated with the LDV measurements was presented previously.[5] The crossflow plane mean V–W measurements presented here are accurate to within ±1% of the upstream crossflow velocity, $U_c = 446$ m/s, at the 95% confidence level and were located within $\pm 0.0125d$ (i.e., ±50 μm) in a measurement grid spaced a distance of $0.125d$ (0.5 mm) in both the spanwise and transverse directions.

Results and Discussion

Figure 2 shows the V–W velocity vectors of half of the crossflow planes at $x/d = 3$ and 5 superimposed on contours of the dimensionless mean streamwise vorticity field $\zeta_x d/U_c$, where

$$\frac{\zeta_x}{U_c/d} = \frac{d}{U_c}\left[\frac{\partial W}{\partial y} - \frac{\partial V}{\partial z}\right] \tag{1}$$

At these x locations, the center-of-rotation velocities are within 2 deg of the streamwise direction. The vorticity fields are dominated by one of the pair of counter-rotating crossflow vortices of the jet plume. At $x/d = 3$, the vorticity contours are roughly kidney shaped, with large gradients near the bottom left and top right of the vortex cross section. These kidney shapes are longest along a line approximately 27 deg from the z axis. At $x/d = 5$, where the vortices have risen away from the wall and moved apart, the vorticity contours have approximately equal radial gradients around their periphery and are roughly elliptical with the major axis aligned with the y direction. This change in the shape of the mean vorticity contours strongly suggests that the motion of each crossflow vortex is, at first, constrained by the other vortex and by the wall and then behaves more as free vortex as it lifts away from the wall. Also, note that for both $x/d = 3$ and 5, the centers of rotation of the in-plane vectors correspond only roughly to the location of maximum $\zeta_x d/U_c$.

The in-plane velocity vectors also show this constraint of the motion of the crossflow vortices. First, in both crossflow planes, the largest measured V–W velocities and in-plane velocity gradients occur in the constrained regions below the vortex center and between the vortex center and the symmetry plane. The unconstrained regions of the vortex (above and outside the vortex center) are much larger and have smaller velocity magnitudes and smaller velocity gradients. As the plume develops from $x/d = 3$ to 5, its cross-sectional area increases mostly in the transverse direction, and the magnitudes and gradients of the in-plane velocities in the constrained regions are significantly reduced. For example, at $x/d = 3$, the largest measured spanwise velocity in the constrained region below the vortex center is $W = -239$ m/s. At $x/d = 5$, the largest measured spanwise velocity in this region is $W = -119$ m/s. Also, note the difference in the spanwise extent of regions of $\zeta_x d/U_c > 0.1$ for the two crossflow planes. The integrated strengths of the crossflow plane vortices at $x/d = 3$ and 5 are 1.11 and 1.00 m^2/s, respectively.[5]

A significant difference between the vortices of this highly three-dimensional and compressible TJISF flowfield and that of a simple, plane, incompressible, two-vortex flowfield is the nature of the

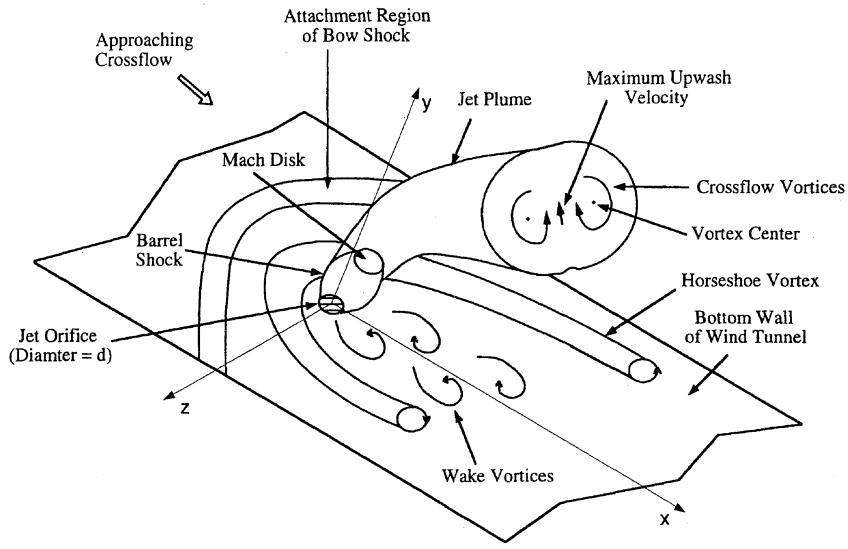

Fig. 1 Schematic of the flowfield of a transverse jet injected into a supersonic flow.

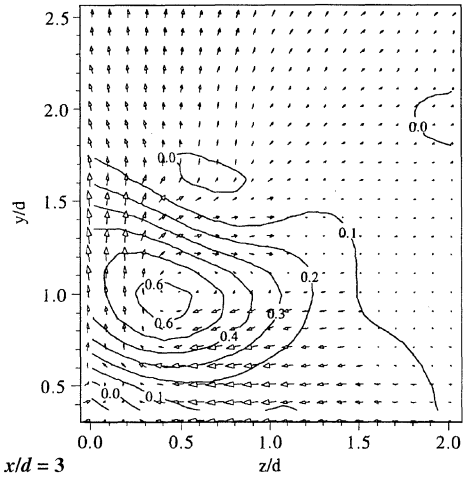

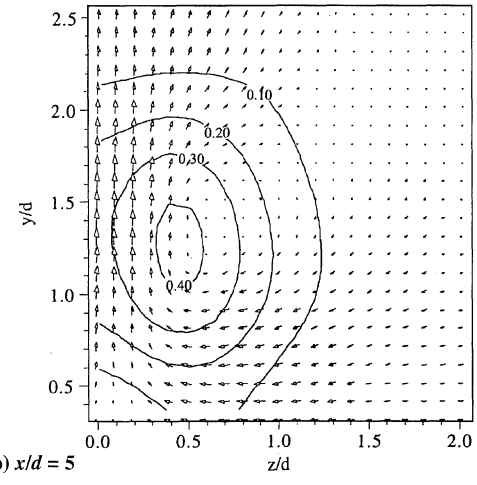

Fig. 2 *V–W* velocity vector field with superimposed streamwise mean vorticity contours: →, 240 m/s.

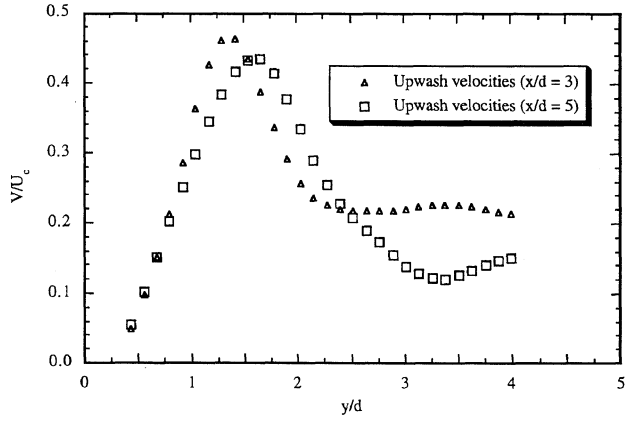

Fig. 3 Upwash velocities at the $z/d = 0$ centerline vs y/d for both crossflow planes.

relatively inviscid velocity field and pressure field surrounding the TJISF jet plume. Upstream of the jet plume and near the wall, the strong normal section of the bow shock creates a subsonic region. Freestream flow velocities (above the boundary layer) increase in the transverse direction because of the curvature of the bow shock. Further from the wall, a three-dimensional slip surface separates the subsonic regions behind the normal section of the bow shock from the supersonic regions downstream of the weaker sections of this shock. Figure 3 shows a plot of the transverse "upwash" velocities, V/U_c, at the $z/d = 0$ centerline vs y/d for the crossflow planes of the current study (see Fig. 1 for the definition and location of the maximum upwash velocity). Unlike those of the subsonic case,[6] these distributions are asymmetric (in y/d) about the location of the maximum upwash velocity. Near the jet wall, the upwash velocities approach zero. Far from the wall, however, the upwash velocities approach the velocity of the crossflow fluid just above the jet plume. In the TJISF flowfield, the crossflow fluid above the plume is downstream of the oblique sections of the bow shock and thus has a significant transverse velocity component. This three-dimensional effect negates the application of simple vortex models, which use upwash velocity distributions to estimate vortex strength,[7] to a jet in supersonic crossflow.

Conclusions

The motion of the counter-rotating, crossflow vortices clearly dominates the downstream velocity field of the TJISF jet plume. The streamwise mean flow vorticity field and the in-plane velocity vectors of the crossflow planes suggest that the motion of each crossflow vortex is, at first, constrained by the other vortex and by the wall. As the vortices move apart and rise away from the wall, the crossflow vortices behave more like two free vortices. This upstream confinement effect, not reported by researchers of low-speed jets, may be associated with the fact that the present flowfield is highly compressible. In some cases, this difference may also be associated with the fact that the jet-to-crossflow momentum flux ratio of the current study is less than that of many of the subsonic transverse jet injection studies performed previously. Another feature of the highly compressible TJISF flowfield is that the profiles of upwash velocities along the $z/d = 0$ centerline vs y/d are asymmetric about the location of maximum upwash velocity. Consequently, the

downstream crossflow vortices are highly three-dimensional, and the use of simple vortex models commonly applied to low-speed jets in crossflow is questionable. Furthermore, because of the upstream constraint of the vortices and the advection of jet fluid caused by the relatively large transverse velocities above the jet plume, the location of maximum upwash velocity is not necessarily expected to occur directly between the vortex centers.

References

[1]Schetz, J. A., and Billig, F. S., "Penetration of Gaseous Jets Injected into a Supersonic Stream," *Journal of Spacecraft and Rockets*, Vol. 3, No. 11, 1966, pp. 1658–1665.

[2]Zukoski, E. E., and Spaid, F. W., "Secondary Injection of Gases into a Supersonic Flow," *AIAA Journal*, Vol. 2, No. 10, 1964, pp. 1689–1696.

[3]Eklund, D. R., Fletcher, D. G., Hartfield, R. J., Jr., McDaniel, J. C., Northam, G. B., Dancey, C. L., and Wang, J. A., "Computational/Experimental Investigation of Staged Injection into a Mach 2 Flow," *AIAA Journal*, Vol. 32, No. 5, 1994, pp. 907–916.

[4]Gallard, R., Geffroy, P., Jacquin, L., and Losfeld, G., "Etude Experimentale sur les Interactions entre un Jet Supersonique Chauffe Transversal et un Ecoulement Supersonique Externe," AGARD Computational and Experimental Assessment of Jets in Crossflow, Winchester, England, UK, April 1993.

[5]Santiago, J. G., "An Experimental Study of the Velocity Field of a Transverse Jet Injected into a Supersonic Crossflow," Ph.D. Thesis, Dept. of Mechanical and Industrial Engineering, Univ. of Illinois at Urbana–Champaign, IL, Aug. 1995.

[6]Andreopoulos, J., and Rodi, W., "Experimental Investigation of Jets in a Crossflow," *Journal of Fluid Mechanics*, Vol. 138, No. 1, 1984, pp. 93–127.

[7]Fearn, R. L., and Weston, R. P., "Vorticity Associated with a Jet in Cross Flow," *AIAA Journal*, Vol. 12, No. 12, 1974, pp. 1666–1671.

F. W. Chambers
Associate Editor

Stiffness Matrix Adjustment Using Incomplete Measured Modes

Ouqi Zhang* and Aspasia Zerva†
Drexel University, Philadelphia, Pennsylvania 19104
and
De-Wen Zhang‡
Beijing Institute of Structure and Environment, Beijing 100076, People's Republic of China

Introduction

THE analytically evaluated dynamic characteristics of a structure seldom agree with the corresponding measured experimental ones. The problem of the correlation between the analytical and measured modal parameters has been addressed for many years, and a number of approaches and discussions have been published on the subject.

In the line of the Baruch/Berman (see Refs. 1–4) and Kabe[5,6] methods, this Technical Note describes a new algorithm for stiffness adjustment. It is shown that the Baruch/Berman method can be considered as a general expression of the adjusted stiffness matrix. The structural connectivity constraints are applied to the generalized Baruch/Berman equation as constraints in the optimal process so that the dimension of the derived governing equation is equal to the number of zero elements in the upper-side triangular part of the stiffness matrix. Generally, the stiffness matrix is obtained from Guyan reduction and is full. Only a few elements with very small values are considered to be zero. In this case, the dimension of the derived governing equation will be relativaly small.

The derived auxiliary equation system is solved by the Householder QR decomposition, which is simple and efficient. A numerical example is presented to illustrate the performance of the method and compare the results with those obtained by the Kabe[5,6] and the Kammer[7] methods.

Method

General Expression for the Adjusted Stiffness Matrix

Given a symmetric positive definite mass matrix $M(n \times n)$ and a rectangular measured modal matrix $\phi_m(n \times m)$, $m \ll n$, which is normalized to fulfill the orthogonality condition

$$\phi_m^t M \phi_m = I \tag{1}$$

where I is the unity matrix and the superscript t denotes matrix transpose. The normalization in Eq. (1) can be achieved by adjusting either the analytical mass matrix (e.g., Ref. 2) or the measured modes (e.g., Refs. 8 and 9) or the approach presented by the writers[10] that requires a smaller change for the measured modes than the method of Refs. 8 and 9.

Assume that $K(n \times n)$ is a symmetric stiffness matrix to be determined that satisfies the eigenvalue equation

$$K\phi_m = M\phi_m \Omega_m^2 \tag{2}$$

where $\Omega_m^2(m \times m)$ represents a diagonal matrix containing the measured system frequencies. If ϕ_h is the matrix of the remaining higher normalized modes of the system defined by M and K, the stiffness matrix will satisfy

$$K = M\phi_h\phi_h^t K\phi_h\phi_h^t M + M\phi_m\phi_m^t K\phi_m\phi_m^t M \tag{3}$$

From Eqs. (1) and (2), we have

$$\phi_m^t K \phi_m = \Omega_m^2 \tag{4}$$

Therefore,

$$K = M\phi_h\phi_h^t K\phi_h\phi_h^t M + M\phi_m\Omega_m^2\phi_m^t M \tag{5}$$

Note that although the unknown normalized higher modal matrix ϕ_h itself depends on the stiffness K, its product $\phi_h\phi_h^t$ can be determined from the given mass matrix and the product of the measured modes,

$$\phi_h\phi_h^t = M^{-1} - \phi_m\phi_m^t \tag{6}$$

Equation (5) is equivalent to Eq. (2). Any stiffness matrix that satisfies Eq. (5) will satisfy Eq. (2), and vice versa. Furthermore, any symmetric matrix used as an initial stiffness matrix in the right-hand side of Eq. (5) will yield an adjusted stiffness matrix that satisfies Eq. (2). Therefore, if K in the right-hand side of Eq. (5) is treated as a variable initial stiffness matrix, indicated by K_0, Eq. (5) becomes the general expression of the adjusted stiffness matrix,

$$K = M\phi_h\phi_h^t K_0\phi_h\phi_h^t M + M\phi_m\Omega_m^2\phi_m^t M \tag{7}$$

It is recognized that the substitution of the analytical stiffness matrix K_a for K_0 into Eq. (7) yields the solution of the Baruch/Berman method.

Generation of the Governing Equation

From Eq. (7) it is concluded that different methods for stiffness matrix adjustment based on Eq. (2) can be interpreted as different choices for the initial stiffness matrix K_0.

As in Ref. 5, we relate the initial stiffness K_0 to the analytical stiffness K_a by

$$K_0 = K_a \otimes \gamma \tag{8}$$

to consider the percentage change of the analytical stiffness elements. In Eq. (13), $\otimes$ represents an element-by-element multipli-

Received June 27, 1996; revision received Feb. 3, 1997; accepted for publication Feb. 10, 1997.

*Research Assistant, Department of Civil and Architectural Engineering. Senior Member AIAA.

†Associate Professor, Department of Civil and Architectural Engineering.

‡Professor. Member AIAA.